AGU100 ADVANCING EARTH AND SPACE SCIENCE

Geophysical Research Letters

RESEARCH LETTER
10.1029/2018GL078139

Special Section:
Cassini's Final Year: Science Highlights and Discoveries

Saturn's Global Zonal Winds Explored by Cassini/VIMS 5-μm Images

Aaron Studwell[1], Liming Li[2], Xun Jiang[1], Kevin H. Baines[3], Patrick M. Fry[4], Thomas W. Momary[3], and Ulyana A. Dyudina[5]

[1]Department of Earth and Atmospheric Sciences, University of Houston, Houston, TX, USA, [2]Department of Physics, University of Houston, Houston, TX, USA, [3]Jet Propulsion Laboratory, California Institute of Technology, Pasadena, CA, USA, [4]Space Science and Engineering Center, University of Wisconsin-Madison, Madison, WI, USA, [5]Space Science Institute, Boulder, CO, USA

Abstract The Cassini Visual and Infrared Mapping Spectrometer (VIMS) 5-μm images are used to derive Saturn's global zonal winds around the 2,000-hPa level. The comparison of zonal winds between 2,000 and 300–500 hPa shows a general consistency of wind structure between the two pressure levels on a global scale. However at some latitudes, the magnitude of the zonal winds differs between these levels. The equatorial zonal winds are stronger downward, while the zonal winds in the middle and high latitudes are generally weaker downward. These new wind measurements also imply that barotropic and baroclinic instabilities probably exist through the relatively deep atmosphere at some latitudes. Finally, our analysis reveals that the VIMS winds in the two polar regions are basically constant with time except for a westerly jet centered at ~88°N, which decreased from 135 ± 7 m/s in 2008 to 91 ± 12 m/s in 2017.

Plain Language Summary Images of giant planets at the visible wavelengths are widely used to track visible clouds and hence estimate the atmospheric winds at the pressure levels of the visible clouds. On the other hand, images at the infrared wavelengths (e.g., 5 μm), which are sensitive to the pressure levels below the visible clouds, can be used to measure the relatively deep winds. Here we use the infrared images recorded by the Cassini spacecraft to measure Saturn's zonal winds (i.e., atmospheric wind in the longitudinal direction) at the relatively deep pressure levels around 2,000 mbar. We provide the global profile of the zonal winds around 2,000 mbar for the first time. The comparison of the global profile of zonal winds between 2,000 mbar and 300–500 mbar reveals interesting characteristics of the vertical shear of zonal winds and the related stabilities on Saturn. In addition, the comparison of the 2,000-mbar zonal winds among different years suggests important temporal characteristics of zonal winds in the polar region of Saturn. This observational study will not only provide key information about the large-scale atmospheric dynamics but also help us develop the theories and models of the general circulation on the giant planets.

Key Points:
- The global profile of zonal winds around 2,000 mbar is generated for the first time; the new profile suggests vertical wind shear
- The vertical shear of zonal winds helps better understand the atmospheric dynamics (e.g., stability)
- Measurements of zonal winds in multiple years suggest the temporal variations of zonal winds in the polar region of Saturn

Supporting Information:
- Supporting Information S1

Correspondence to:
L. Li,
lli7@central.uh.edu

Citation:
Studwell, A., Li, L., Jiang, X., Baines, K. H., Fry, P. M., Momary, T. W., & Dyudina, U. A. (2018). Saturn's global zonal winds explored by Cassini/VIMS 5-μm images. *Geophysical Research Letters*, *45*. https://doi.org/10.1029/2018GL078139

Received 29 MAR 2018
Accepted 29 JUN 2018
Accepted article online 6 JUL 2018

1. Introduction

Wind fields play a critical role in the meteorology and climate of planetary atmospheres by setting the basic environment for atmospheric dynamical processes, such as storms, vortices, and waves (e.g., Batchelor, 1967; Holton, 2004; Pedlosky, 1987). Large-scale zonal winds, defined as the easterly or westerly winds averaged over different longitudes in a latitude bin, are very strong (~100–400 m/s) on the four giant planets (i.e., Jupiter, Saturn, Uranus, and Neptune). Multi-instrument observations of Saturn from the Cassini spacecraft acquired over 14 years (2004–2017) provide a unique opportunity to explore the spatiotemporal variability of the zonal winds on Saturn.

The continuum band images recorded by the Cassini Imaging Science Subsystem (ISS; Porco et al., 2004) have been widely used to explore Saturn's zonal winds at the same level as the top visible clouds (e.g., Antuñano et al., 2015; Del Genio et al., 2007; Del Genio & Barbara, 2012; Dyudina et al., 2008, 2009; Garcia-Melendo et al., 2010; Garcia-Melendo, Perez-Hoyos, et al., 2011; Li et al., 2011; Porco et al., 2005; Sanchez-Lavega et al., 2016; Sayanagi et al., 2013; Vasavada et al., 2006). The top visible clouds on Saturn are generally referred to as the ammonia clouds (e.g., West, 1983), residing around the 300–500 hPa pressure level (e.g., Perez-Hoyos & Sanchez-Lavega, 2006a; Tomasko & Doose, 1984; West, 1983). The ISS zonal winds can be further used to explore the wind patterns above the visible clouds by combining the atmospheric temperature data

retrieved from the Cassini Composite and InfraRed Spectrometer (CIRS; Flasar, Kunde, Abbas, et al., 2004) and the thermal wind relationship (e.g., Achterberg et al., 2014; Flasar et al., 2005; Fletcher et al., 2010, 2011, 2016, 2017; Fouchet et al., 2008; Guerlet et al., 2011; Li et al., 2007, 2008, 2011, 2013; Read et al., 2007; Read, Conrath, et al., 2009).

The observations from the Cassini ISS/CIRS improve our understanding of the zonal winds within and above the ammonia clouds around 300–500 hPa. Conversely, the infrared images can be used to explore the zonal winds below the ammonia clouds. In particular, the images around 5 μm recorded by the Cassini Visual and Infrared Mapping Spectrometer (VIMS; Brown et al., 2004) are sensitive to the pressure levels around 2,000 hPa (Baines et al., 2005, 2009; Momary et al., 2006). Therefore, the Cassini VIMS 5-μm images have been used to explore Saturn's zonal winds at the relatively deep levels in recent years (Baines et al., 2005, 2009; Choi et al., 2009; Dyudina et al., 2009). However, a systematic analysis of the global profile of VIMS 5-μm winds is not available yet, partly because such an analysis would require high-spatial-resolution pole-to-pole observations. In addition, the temporal variations of VIMS 5-μm zonal winds have not been explored either. Here, we present a study of the global profile of VIMS 5-μm zonal winds and an initial analysis of the temporal variations of zonal winds by combining the Cassini VIMS observations in multiple years

2. Results

The VIMS instrument is a color camera that captures images in 352 different wavelengths, ranging from ~ 0.35 to ~ 5.1 μm (Brown et al., 2004). Here we mainly use the VIMS images recorded around 5 μm to measure the zonal winds around 2,000 hPa. The techniques of data processing (Baines et al., 2005, 2009; Barnes et al., 2007; Gaddis et al., 1997; Sromovsky & Fry, 2010), the methods of measuring the zonal winds (Baines et al., 2005, 2009; Dyudina et al., 2008, 2009; Li et al., 2004, 2011; Limaye, 1986), and the uncertainty estimates (Baines et al., 2009; Dyudina et al., 2009; Garcia-Melendo, Perez-Hoyos, et al., 2011; Li et al., 2004) are introduced in the supporting information.

An understanding of Saturn's rotation period, which is used as a reference for the measurements of zonal winds, is important. The Voyager observations (Desch & Kaiser, 1981) suggest a rotation period of 10 hr 39 min 24 s for Saturn. The new Cassini observations suggest shorter rotation periods: 10 hr 32 min 35 s (Anderson & Schubert, 2007) or 10 hr 34 min 13 s (Read, Dowling, & Schubert, 2009). To be consistent with our wind measurements based on the Cassini observations, this study uses the rotation periods from the Cassini observations (Anderson & Schubert, 2007; Read, Dowling, & Schubert, 2009). A rotation period of 10 hr 33 min 24 s is used in the wind profiles determined by this study, which is an average of the two Cassini values (10 hr 32 min 35 s and 10 hr 34 min 13 s). For comparison, the global profiles of zonal winds referred with the old Voyager rotation period (10 hr 39 min 24 s) are also plotted in Figure 1.

Figure 1 displays the global profile of the VIMS 5-μm zonal winds around 2,000 hPa, which is compared with the global profile of the Cassini ISS continuum band zonal winds around 300–500 hPa. The VIMS 46 and ISS wind profiles shown in Figure 1 are from different times (VIMS winds mainly in 2015–16 and ISS winds mainly in 2004–08), but previous studies (e.g., Garcia-Melendo et al., 2011; Li et al., 2011; Sanchez-Lavega et al., 2016) suggest that the ISS zonal winds around 300-500 hPa did not significantly change with time during the Cassini period The investigations of the temporal variation of the VIMS zonal winds are lacking. Therefore, we cannot rule out the possibility that the difference between the two wind profiles shown in Figure 1 is due to temporal variations, even though it is more likely that the difference is due to the vertical shear of zonal winds on Saturn because the VIMS images and the ISS images probe different pressure levels.

Figure 1 shows a global-scale consistency between the VIMS and ISS profiles, which suggests that the VIMS zonal winds around 2,000 hPa have the basically same structures as those of the ISS zonal winds around 300–500 hPa. However, there are significant differences between the two profiles at some latitudes. These differences are greater than the estimated uncertainties, which suggests that they are statistically robust. One of the significant differences is noted in the equatorial region (i.e., 5°S–5°N) in which the VIMS winds are stronger than the ISS winds by approximately 50 m/s. Previous measurements of the VIMS zonal winds in 2004–2008 (Choi et al., 2009), which have the roughly same time frame as the ISS wind profile (Figure 1), suggest even stronger equatorial winds. Therefore, we think the equatorial zonal winds are

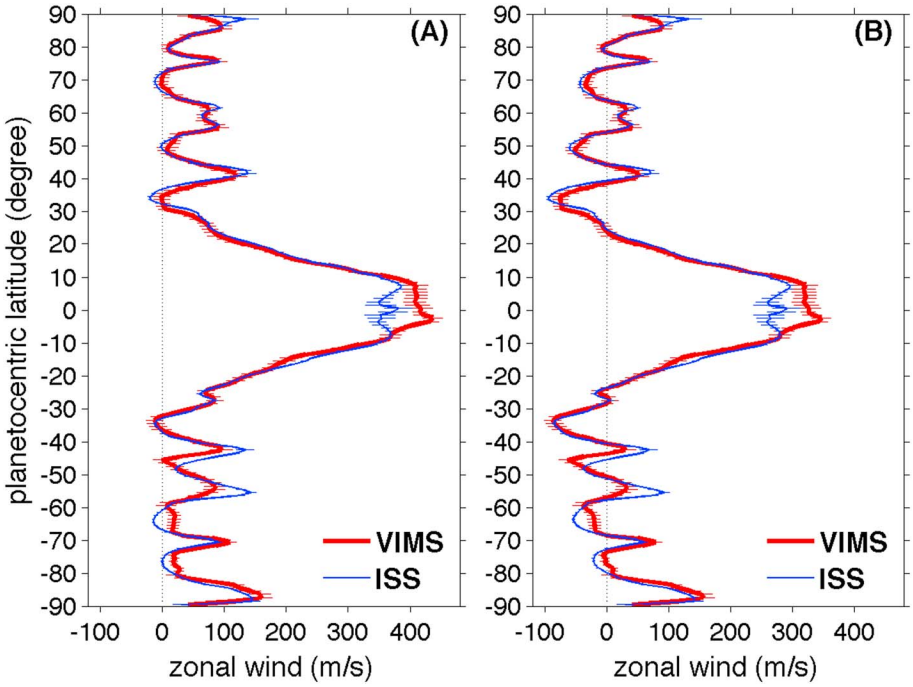

Figure 1. Comparison of global profile between the VIMS zonal winds and the ISS zonal winds. (a) Wind profiles based on the Voyager rotation period ~ 10 hr 39 min 24 s (Desch & Kaiser, 1981). (b) Wind profiles based on the average Cassini rotation period ~ 10 hr 33 min 24 s (Anderson & Schubert, 2007; Read, Dowling, & Schubert, 2009). The horizontal lines represent error bars. The global profile of the VIMS 5-μm zonal winds mainly comes from the VIMS observations in 2015–2017 (Table S1) except for 89–89.5°S from the VIMS observations in 2006 (Dyudina et al., 2009). The global profile of the ISS zonal winds comes from the ISS observations in 2004–2008 (Garcia-Melendo, Perez-Hoyos, et al., 2011) except for 83–89.5°N from the ISS observations in 2013 (Antuñano et al., 2015). VIMS = Visual and Infrared Mapping Spectrometer; ISS = Imaging Science Subsystem.

stronger by at least 50 m/s at the 2,000 hPa pressure level than at the 300–500 hPa pressure level, which is consistent with the analysis in a previous study (Sanchez-Lavega et al., 2016).

The VIMS observations suggest that the equatorial zonal winds become stronger when going deeper from the visible clouds around 300–500 hPa. Another point of interest is to determine how the vertical shear of the equatorial zonal winds varies above the visible clouds. Based on the Cassini/CIRS retrieved temperature, Flasar et al. (2005) and Li et al. (2008) suggest that the equatorial zonal winds basically decay from the pressure level of visible clouds (~ 300–500 hPa) to the tropopause (~ 50 hPa). Such a decay is confirmed by an investigation based on the observations using the Cassini ISS strongest methane filter (Li et al., 2011). Therefore, it seems that Saturn's equatorial zonal winds keep increasing from the tropopause, which is around 50 hPa (Fletcher et al., 2010), to the 2,000 hPa pressure level. Such a picture is qualitatively similar to the vertical variation of Jupiter's equatorial zonal winds measured by the Galileo Probe (Atkinson, 2001; Atkinson et al., 1996, 1997, 1998) and the Cassini spacecraft (Flasar, Kunde, Achterberg, et al., 2004; Li et al., 2006; Simon et al., 2015; Simon-Miller et al., 2006), in which Jupiter's equatorial zonal winds keep increasing from the tropopause ~ 100 hPa to the pressure level around 5,000 hPa.

The VIMS profile in Figure 1 also displays a north-south asymmetry of Saturn's equatorial zonal winds. Jupiter's equatorial zonal winds at the pressure level of visible clouds also have such a latitudinal asymmetry, which is possibly related to the north equatorial plumes via Rossby wave activities (e.g., Allison et al., 1995; Garcia-Melendo, Arregi, et al., 2011). The VIMS maps (e.g., Figure S1) show a semiregular spacing of longitudinal features a few degrees north of the equator. Such features are possibly responsible for the latitudinal asymmetry of the VIMS equatorial zonal winds shown in Figure 1, but further analysis is needed.

Figure 1 further suggests that the VIMS zonal winds and the ISS zonal winds are basically consistent in the latitude range from 40°S to 25°N except for the equatorial zonal winds between 5°S and 5°N. In the higher

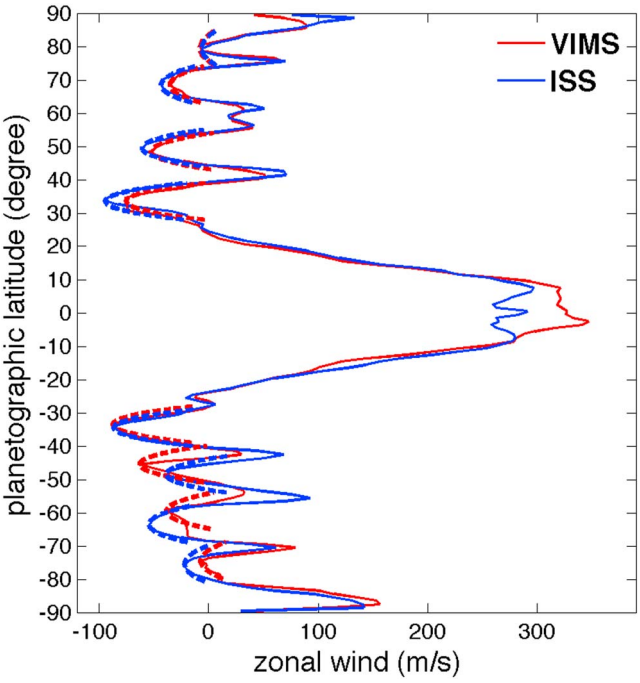

Figure 2. Curvature U_{yy} of the zonal wind profiles compared to β. The parabolic curves are defined by $U_{yy} = \beta$ and are centered on the westward jet maxima. Red and blue dashed parabolas are for the Visual and Infrared Mapping Spectrometer (VIMS) and Imaging Science Subsystem (ISS) wind profiles, respectively. Where the measured wind profile lies inside the parabola, the flow violates the barotropic stability criterion.

latitudes, Figure 1b shows that the magnitudes of the VIMS zonal winds around 2,000 hPa are generally smaller than those of the ISS zonal winds around 300–500 hPa for both easterly jets (e.g., 77°S, 61–64°S, 34°N, 50°N, and 69°N) and westerly jets (e.g., 55°S, 43°S, 42°N, 61°N, and 87–89°N). However, the easterly jet around 44–48°S is stronger at the 2,000 hPa pressure level than at the 300–500 hPa pressure level. In addition, the westerly jets around 86°S, 70°S, and 76°N and the easterly jet around 79°N show the roughly consistent magnitudes of zonal winds between the VIMS and ISS profiles. The consistent westerly jet around 76°N has roughly the same position with that of the polar hexagon, which probably suggests that the hexagon is a propagating Rossby wave (Allison et al., 1990; Baines et al., 2009).

Figure 1 suggests that a majority of the zonal jets in the middle and high latitudes become weaker from the 300–500 hPa pressure level to the 2,000 hPa pressure level. Such a vertical shear of zonal winds in the middle and high latitudes is opposite to that in the equatorial region (5°S–5°N), in which the zonal winds are stronger at 2,000 hPa than at 300–500 hPa. It should be mentioned that it is also possible that the differences of zonal winds in the middle and high latitudes between the two pressure levels are due to the temporal variations, even though previous studies of the ISS winds (Garcia-Melendo, Perez-Hoyos, et al., 2011; Li et al., 2011; Sanchez-Lavega et al., 2016) and our examination of the temporal variations of the VIMS winds (Figure 4) suggest that both of the ISS and VIMS zonal winds are likely stable over time in most latitudes.

Based on the wind profiles in Figure 1, we can discuss the atmospheric stability. The total vorticity for a barotropic atmosphere, in which zonal winds are dominant, can be expressed as the sum of the planetary vorticity (i.e., Coriolis parameter *f*) and the relative vorticity of zonal winds ($-U_y = -\partial U/\partial y$). Then the barotropic stability can be shown as the gradient of the total vorticity (β–U_{yy}, where $\beta = \partial f/\partial y$ and $-U_{yy} = -\partial^2 U/\partial y^2$). The barotropic stability criterion suggests that flows are stable when $\beta - U_{yy} > 0$. When $\beta - U_{yy} < 0$, the flows violate the criterion, and perturbations (e.g., waves, eddies, vortices, and turbulences) can develop. The meridional gradient of the planetary vorticity β is positive everywhere. The U_{yy} in the gradient of relatively vorticity ($-U_{yy}$) actually represents the curvature of zonal jets. Only easterly jets have positive curvature ($U_{yy} > 0$), so that the stability criterion can possibly be violated ($\beta - U_{yy} < 0$). WE plot parabolas with curvature β that are centered on the easterly jets in Figure 2, which follows a similar analysis of Jupiter's zonal winds (Li et al., 2004). When the easterly jets are sharper than the parabolas ($U_{yy} > \beta$), the jets violated the barotropic stability criterion.

For the Cassini ISS profile, Figure 2 shows that the easterly jets around 64°S, 33°S, 34°N, 50°N, and 69°N are a little bit sharper than the corresponding parabolas with curvature β, which suggests that these jets are marginally unstable from the barotropic perspective. On the other hand, the easterly jets around 77°S, 48°S, and 79°N are much sharper than the corresponding parabolas with curvature β, which implies that these jets are very unstable. Basically, all easterly jets are barotropically unstable, which can help explain why Saturn's vortices are concentrated around these latitudes of easterly jets (Trammell et al., 2014, 2016). The VIMS profile in Figure 2 shows that the VIMS easterly jets have similar sharpness with that of the ISS easterly jets except for the VIMS jets around 46°S and 59°S. The two VIMS easterly jets are significantly sharper than the corresponding ISS jets, which suggests that the two easterly jets are more unstable at 2,000 hPa than at 300–500 hPa.

Saturn's zonal winds probably keep stable with time at most latitudes with violating the barotropic criterion near the peaks of some easterly jets, which probably suggests that the zonal winds are baroclinic (Li et al., 2004). The atmospheric baroclinicity is related to the vertical shear of winds. Therefore, the two wind profiles at different pressure levels in Figure 1 can be used to examine the vertical shear of zonal winds and hence the baroclinic stability (e.g., Holton, 2004). First, we use the vertical shear of zonal winds to examine the Richardson number, which is closely related to the atmospheric stratification, turbulence development,

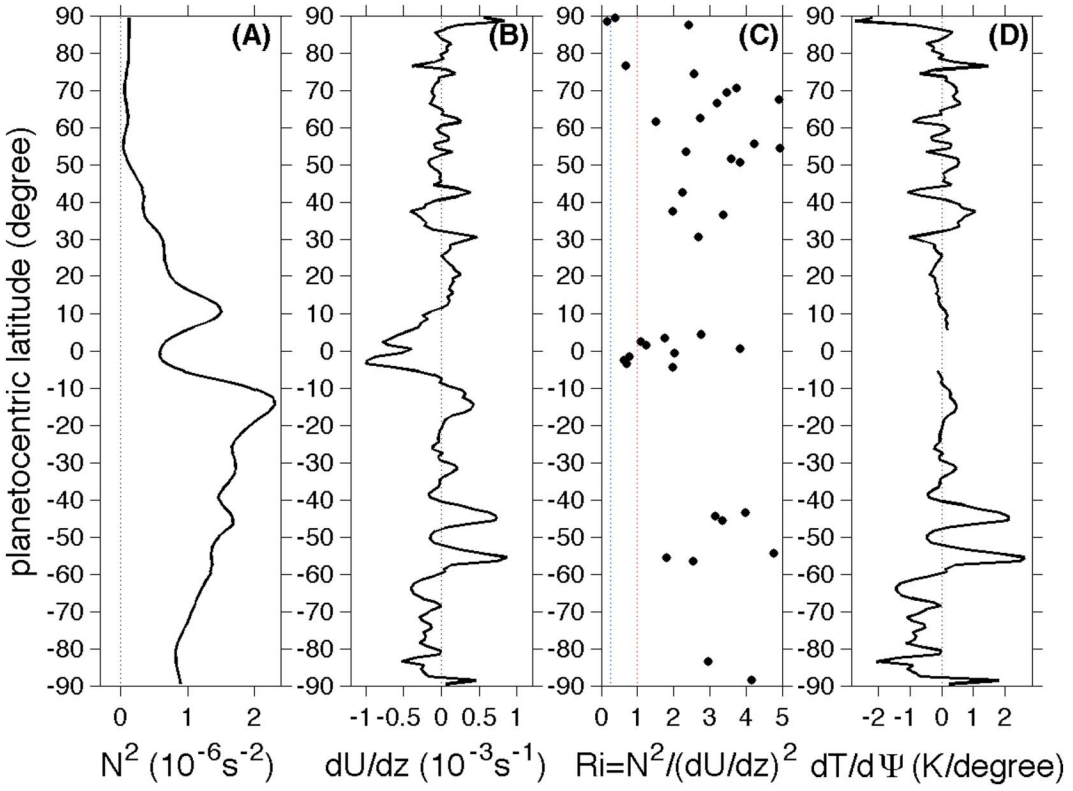

Figure 3. Static stability, vertical shear of zonal winds, Richardson number, and estimated meridional temperature gradient. (a) Static stability N^2. (b) Vertical shear of zonal winds dU/dz. (c) Richardson number Ri. (d) Meridional temperature gradient dT/dΨ. In panel c, the blue and red vertical lines stand for Ri = 1/4 and Ri = 1, respectively. Only latitudes with Richardson numbers less than 5 are plotted in panel c. At some latitudes in which the vertical shear of zonal winds is very small, the values of Richardson number are extremely large (>1,000). In panel d, the very narrow latitude band around the equator (5°S–5°N), in which the classical thermal wind equation does not work (Batchelor, 1967; Pedlosky, 1987), is left blank.

and baroclinic instability (e.g., Allison et al., 1995; Holton, 2004). The Richardson number can be expressed as $Ri = N^2/(\mathrm{d}U/\mathrm{d}z)^2$, where N is the buoyancy frequency and dU/dz is the vertical shear of zonal winds.

We first compute the static stability N^2 based on Saturn's temperature retrieved by the Cassini CIRS (Figure 3a). We use the CIRS temperature in 2008 from a previous study (Fletcher et al., 2010). The CIRS-retrieved temperature data are robust above the 500 hPa pressure level (Flasar, Kunde, Abbas, et al., 2004; Fletcher et al., 2010), so we compute N^2 at 500 hPa to represent the static stability in the pressure range from 300–500 to 2,000 hPa. The central difference scheme and the CIRS-retrieved temperature at 470 and 550 hPa, which are two pressure levels close to the reference level at 500 mbar, are used to compute the static stability N^2 at 500 hPa. Then the difference of zonal winds between the VIMS and ISS profiles (Figure 1) is used to estimate the vertical shear of zonal winds dU/dz (Figure 3b). Based on the static stability N^2 and the vertical shear of zonal winds dU/dz, we can compute the Richardson number Ri (Figure 3c). We also use the thermal wind relationship to estimate the meridional temperature gradient in the pressure range from 300–500 mbar to 2,000 hPa. The thermal wind relationship (Batchelor, 1967; Flasar et al., 2005; Li et al., 2007; Pedlosky, 1987) can be expressed as $\mathrm{d}U/\mathrm{d}z = (-\rho \mathrm{Rg}/fP)(\mathrm{d}T/r\mathrm{d}\Psi)$, where ρ is density, R is Saturn's gas constant, P is pressure, r is Saturn's radius, and Ψ is latitude. So we have the meridional temperature gradient as $\mathrm{d}T/\mathrm{d}\Psi = (-rfP/\rho \mathrm{Rg})(\mathrm{d}U/\mathrm{d}z)$. Here we use the density at 1,000 hPa (ρ = 0.19 kg/m^3), which comes from the NASA Space Science Data Coordinated Archive (https://nssdc.gsfc.nasa.gov/planetary/factsheet/saturnfact.html), to represent the average atmospheric density in the pressure range from 300–500 to 2,000 hPa. The estimated meridional temperature gradient dT/dΨ is shown in Figure 3d. It should be cautioned that the vertical shear of zonal winds and the related parameters shown in Figure 3 are rough estimates, because we assume that the zonal winds linearly change from 300–500 to 2,000 hPa.

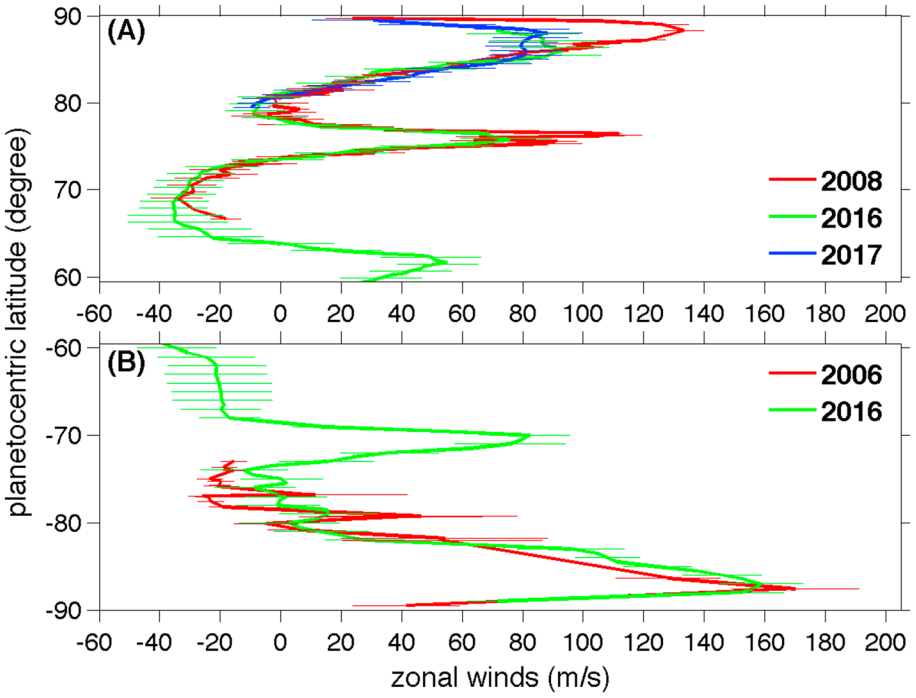

Figure 4. Comparison of the Visual and Infrared Mapping Spectrometer 5-μm zonal winds among different years in the two polar regions. (a) The northern polar region. (b) The southern polar region. The horizontal lines represent error bars. The zonal winds before 2016 come from two previous studies, in which the 2008 zonal winds in the northern polar region come from a study by Baines et al. (2009) and the 2006 zonal winds in the southern polar region comes from the study by Dyudina et al. (2009). Please note that all wind profiles based on the Cassini average rotation period ~ 10 hr 33 min 24 s (Anderson & Schubert, 2007; Read, Dowling, & Schubert, 2009).

Figure 3a shows that the static stability is positive everywhere, which suggests that Saturn's atmosphere is convectively stable. The panel also shows that the static stability is larger in the southern hemisphere than in the northern hemisphere, which is related to the seasonal change on Saturn. The temperature used for computing N^2 comes from 2008 (Fletcher et al., 2010), which is the summer of the southern hemisphere. In summer, the warmer upper atmosphere due to the solar heating (Perez-Hoyos & Sanchez-Lavega, 2006b) probably results in large static stability. A minimum of static stability appears around the equator, which implies that Saturn's equatorial region possibly favors convection.

Figure 3b suggests that Saturn's equatorial region has largely negative vertical shear of zonal winds. In addition, both positive and negative vertical wind shears show up in the middle latitudes, as well as near the north pole. Figure 3c further shows that the values of R_i are smaller than 1 around the equator and the northern polar region, which suggests that one necessary condition for the baroclinic instability is satisfied over there (Allison et al., 1995; Holton, 2004). The values of R_i are even close or smaller than 1/4 near the North Pole, which implies that the vertical shear of zonal winds is probably strong enough to sustain turbulence (Holton, 2004). Figure 3d is the estimated meridional temperature gradient for the relatively deep atmosphere in the pressure range from 300–500 mbar to 2,000 hPa. The thermal wind relationship suggests that the meridional temperature gradient is proportional to the vertical shear of zonal winds. Therefore, these latitudes with the largely positive/negative vertical shear of zonal winds have significant temperature gradients. In some latitudes, the meridional temperature gradient can reach a couple of kelvins per degree (e.g., 45°S, 56°S, and 89°N). However, the equatorial region is an exception, in which the temperature gradient is small even though the largely negative vertical shear of zonal winds exists. The main reason is that the Coriolis parameter is very small in the equatorial region, so the meridional temperature gradient must be small to keep the balance for the thermal wind relationship.

Finally, we conduct an initial analysis of temporal variations of the VIMS 5-μm zonal winds based on the Cassini observations in multiple years. Figure 4 displays the zonal winds in the two polar regions based on

the observations during the period of 2016–2017. The new measurements in 2016–2017 are further compared with previous measurements in 2006 and 2008 (Baines et al., 2009; Dyudina et al., 2009). This figure shows that the difference of the VIMS zonal winds among different years are smaller than the uncertainties of measurements for most latitudes except for the latitudinal range of 85–90°N. The zonal jet centered at ~ 88°N experienced significant decrease at 44 ± 14 m/s (33 ± 14%) from 135 ± 7 m/s in 2008 to 91 ± 12 m/s in 2017. The results shown in Figure 4 are limited to high latitudes and do not cover all years of the Cassini observations. A systematic analysis of the VIMS zonal winds across all latitudes and during the complete Cassini period (2004–2017) will shed more light on the temporal variations of the VIMS zonal winds on Saturn.

3. Conclusions and Discussions

In this study, we provide an analysis of the spatiotemporal variations of the relatively deep zonal winds with the Cassini VIMS observations. The first global profile of the zonal winds around the 2,000 hPa pressure level is generated. The comparison between the VIMS zonal wind and the ISS zonal wind profiles suggests a consistency of wind structure on a global scale. However, significant differences between the two wind profiles are identified at some latitudes. In particular, the equatorial region from 5°S to 5°N shows an increase in wind speed by at least 50 m/s from 300–500 to 2,000 hPa. Conversely, a decrease of wind speed from 300–500 to 2,000 hPa exists for most zonal jets in middle and high latitudes.

The zonal winds at the two pressure levels (300–500 and 2,000 hPa) are further used to investigate the atmospheric stability, which suggests that most zonal jets in the two pressure levels are barotropically unstable. The investigation of Richardson number further suggests that one necessary condition for the baroclinic instability is satisfied in these latitudes with significant vertical shear of zonal winds. Finally, the thermal wind relationship suggests that the meridional temperature gradient in the pressure range from 300–500 to 2,000 hPa can reach a couple of kelvins per degree at some middle and high latitudes.

The Cassini observations in different years are used to explore the temporal variations of the VIMS 5-μm zonal winds, which suggests that the VIMS 5-μm zonal winds were basically constant from 2006 to 2017 in the two polar regions except for the latitude range of 85–90°N where a westerly jet decreased ~ 44 ± 14 m/s from 2008 to 2017.

This paper is an initial study of a systematic analysis characterizing the spatiotemporal variations of Saturn's zonal winds with the long-term (2004–2017) multi-instrument observations (i.e., CIRS, ISS, and VIMS). First, the current study mainly focuses on the recent three years (2015–2017) even though some previous measurements are discussed. Therefore, only one global profile of the VIMS 5-μm zonal winds is provided. In principle, we can get multiple global profiles of the VIMS 5-μm zonal winds based on the Cassini long-term (2004–2017) observations. Multiple global profiles will make it possible to explore the temporal variations of the relatively deep zonal winds around 2,000 hPa not only in the polar region but also in other latitudes. Second, the combinations of the VIMS measurements with the investigations of zonal winds by the ISS and CIRS will help us get a more complete picture of the vertical structure of Saturn's zonal winds not only below but also above the visible ammonia clouds.

Acknowledgments
We acknowledge the Cassini VIMS team for recording the raw data sets. We also acknowledge the support from the NASA ROSES CDAP and PDART programs. Finally, we acknowledge the two anonymous reviewers who provided constructive suggestions. The Cassini data sets used in this paper are available at the Planetary Data System of the National Aeronautics and Space Administration (http://pds.nasa.gov/).

References

Achterberg, R. K., Gierasch, P. J., Conrath, B. J., Fletcher, L. N., Hesman, B. E., Bjoraker, G. L., & Flasar, F. M. (2014). Changes to Saturn's zonal-mean tropospheric thermal structure after the 2010–2011 northern hemisphere storm. *The Astrophysical Journal*, *786*(2), 92. https://doi.org/10.1088/0004-637X/786/2/92

Allison, M., Del Genio, A. D., & Zhou, W. (1995). Richardson number constraints for the Jupiter and outer planet wind regime. *Geophysical Research Letters*, *22*(21), 2957–2960. https://doi.org/10.1029/95GL02818

Allison, M., Godfrey, D. A., & Beebe, R. F. (1990). A wave dynamical interpretation of Saturn's polar hexagon. *Science*, *247*(4946), 1061–1063. https://doi.org/10.1126/science.247.4946.1061

Anderson, J. D., & Schubert, G. (2007). Saturn's gravitational field, internal rotation, and interior structure. *Science*, *317*(5843), 1384–1387. https://doi.org/10.1126/science.1144835

Antuñano, A., Río-Gaztelurrutia, T., Sánchez-Lavega, A., & Hueso, R. (2015). Dynamics of Saturn's polar regions. *Journal of Geophysical Research: Planets*, *120*, 155–176. https://doi.org/10.1002/2014JE004709

Atkinson, D. H. (2001). The Galileo Jupiter probe Doppler wind experiment. *Solar System Research*, *35*(5), 354–375. https://doi.org/10.1023/A:1012348103693

Atkinson, D. H., Ingersoll, A. P., & Seiff, A. (1997). Deep winds on Jupiter as measured by the Galileo probe. *Nature*, *388*(6643), 649–650. https://doi.org/10.1038/41718

Atkinson, D. H., Pollack, J. B., & Seiff, A. (1996). Galileo Doppler measurements of the deep zonal winds at Jupiter. *Science*, *272*(5263), 842–843. https://doi.org/10.1126/science.272.5263.842

Atkinson, D. H., Pollack, J. B., & Seiff, A. (1998). The Galileo probe Doppler wind experiment: Measurement of the deep zonal winds on Jupiter. *Journal of Geophysical Research*, *103*(E10), 22,911–22,928. https://doi.org/10.1029/98JE00060

Baines, K. H., Momary, T. W., Fletcher, L. N., Showman, A. P., Roos-Serote, M., Brown, R. H., et al. (2009). Saturn's north polar cyclone and hexagon at depth revealed by Cassini/VIMS. *Planetary and Space Science*, *57*(14-15), 1671–1681. https://doi.org/10.1016/j.pss.2009.06.026

Baines, K. H., Momary, T. W., & Roos-Serote, M. (2005). The deep winds of Saturn: First measurements of the zonal windfield near the two-bar level. *Bulletin of the American Astronomical Society*, *37*, 658.

Barnes, J. W., Brown, R. H., Soderblom, L., Buratti, B. J., Sotin, C., Rodriguez, S., et al. (2007). Global-scale surface spectral variations on Titan seen from Cassini/VIMS. *Icarus*, *186*(1), 242–258. https://doi.org/10.1016/j.icarus.2006.08.021

Batchelor, G. K. (1967). *An introduction to fluid dynamics*. London: Cambridge University Press.

Brown, R. H., Baines, K. H., Bellucci, G., Bibring, J. P., Buratti, B. J., Capaccioni, F., et al. (2004). The Cassini Visual and Infrared Mapping Spectrometer (VIMS) investigation. *Space Science Reviews*, *115*(1-4), 111–168. https://doi.org/10.1007/s11214-004-1453-x

Choi, D. S., Showman, A. P., & Brown, R. H. (2009). Cloud features and zonal wind measurements of Saturn's atmosphere as observed by Cassini/VIMS. *Journal of Geophysical Research*, *114*, E04007. https://doi.org/10.1029/2008JE003254

Del Genio, A. D., & Barbara, J. M. (2012). Constraints on Saturn's tropospheric general circulation from Cassini ISS images. *Icarus*, *219*(2), 689–700. https://doi.org/10.1016/j.icarus.2012.03.035

Del Genio, A. D., Barbara, J. M., Ferrier, J., Ingersoll, A. P., West, R. A., Vasavada, A. R., et al. (2007). Saturn eddy momentum fluxes and convection: First estimates from Cassini images. *Icarus*, *189*, 479–492.

Desch, M. D., & Kaiser, M. L. (1981). Voyager measurement of the rotation period of Saturn's magnetic-field. *Geophysical Research Letters*, *8*(3), 253–256. https://doi.org/10.1029/GL008i003p00253

Dyudina, U. A., Ingersoll, A. P., Ewald, S. P., Vasavada, A. R., West, R. A., Baines, K. H., et al. (2009). Saturn's south polar vortex compared to other large vortices in the solar system. *Icarus*, *202*(1), 240–248. https://doi.org/10.1016/j.icarus.2009.02.014

Dyudina, U. A., Ingersoll, A. P., Ewald, S. P., Vasavada, A. R., West, R. A., del Genio, A. D., et al. (2008). Dynamics of Saturn's south polar vortex. *Science*, *319*(5871), 1801–1801. https://doi.org/10.1126/science.1153633

Flasar, F. M., Achterberg, R. K., Conrath, B. J., Pearl, J. C., Bjoraker, G. L., Jennings, D. E., et al. (2005). Temperatures, winds, and composition in the Saturnian system. *Science*, *307*(5713), 1247–1251. https://doi.org/10.1126/science.1105806

Flasar, F. M., Kunde, V. G., Abbas, M. M., Achterberg, R. K., Ade, P., Barucci, A., et al. (2004). Exploring the Saturn system in the thermal infrared: The composite infrared spectrometer. *Space Science Reviews*, *115*(1-4), 169–297. https://doi.org/10.1007/s11214-004-1454-9

Flasar, F. M., Kunde, V. G., Achterberg, R. K., Conrath, B. J., Simon-Miller, A. A., Nixon, C. A., et al. (2004). An intense stratospheric jet on Jupiter. *Nature*, *427*(6970), 132–135. https://doi.org/10.1038/nature02142

Fletcher, L. N., Achterberg, R. K., Greathouse, T. K., Orton, G. S., Conrath, B. J., Simon-Miller, A. A., et al. (2010). Seasonal change on Saturn from Cassini/CIRS observations, 2004-2009. *Icarus*, *208*(1), 337–352. https://doi.org/10.1016/j.icarus.2010.01.022

Fletcher, L. N., Guerlet, S., Orton, G., Cosentino, R., Fouchet, T., Irwin, P., et al. (2017). Disruption of Saturn's quasi-periodic equatorial oscillation by the great northern storm. *Nature Astronomy*, *1*, 765–770. https://doi.org/10.1038/s41550-017-0271-5,2017

Fletcher, L. N., Hesman, B. E., Irwin, P. G. J., Baines, K. H., Momary, T. W., Sanchez-Lavega, A., et al. (2011). Thermal structure and dynamics of Saturn's northern springtime disturbance. *Science*, *332*(6036), 1413–1417. https://doi.org/10.1126/science.1204774

Fletcher, L. N., Irwin, P. G., Achterberg, R. K., Orton, G. S., & Flasar, F. M. (2016). Seasonal variability of Saturn's tropospheric temperatures, winds and Para-H_2 from Cassini far-IR spectroscopy. *Icarus*, *264*, 137–159. https://doi.org/10.1016/j.icarus.2015.09.009

Fouchet, T., Guerlet, S., Strobel, D. F., Simon-Miller, A. A., Bezard, B., & Flasar, F. M. (2008). An equatorial oscillation in Saturn's middle atmosphere. *Nature*, *453*(7192), 200–202. https://doi.org/10.1038/nature06912

Gaddis, L., Hawke, B. R., & Robinson, M. S. (1997). Analyses of three classes of small lunar pyroclastic deposits with Clementine data. *Lunar and Planetary Science*, *XXVIII*, 389–390.

Garcia-Melendo, E., Arregi, J., Rojas, J. F., Hueso, R., Barrado-Izagirre, N., Gómez-Forrellad, J. M., et al. (2011). Dynamics of Jupiter's equatorial region at cloud top level from Cassini and HST images. *Icarus*, *211*(2), 1242–1257. https://doi.org/10.1016/j.icarus.2010.11.020

Garcia-Melendo, E., Perez-Hoyos, S., Sanchez-Lavega, A., Legarreta, J., & Hueso, R. (2011). Saturn's zonal wind profile in 2004–2009 from Cassini ISS images and its long-term variability. *Icarus*, *215*(1), 62–74. https://doi.org/10.1016/j.icarus.2011.07.005

Garcia-Melendo, E., Sanchez-Lavega, A., Legarreta, J., Perez-Hoyos, S., & Hueso, R. (2010). A strong high altitude narrow jet detected at Saturn's equator. *Geophysical Research Letters*, *37*, L22204. https://doi.org/10.1029/2010GL045434

Guerlet, S., Fouchet, T., Bézard, B., Flasar, F. M., & Simon-Miller, A. A. (2011). Evolution of the equatorial oscillation in Saturn's stratosphere between 2005 and 2010 from Cassini/CIRS limb data analysis. *Geophysical Research Letters*, *38*, L09201. https://doi.org/10.1029/2011GL047192

Holton, J. R. (2004). *An introduction to dynamic meteorology* (4th ed.). San Diego, CA: Academic.

Li, L., Achterberg, R. K., Conrath, B. J., Gierasch, P. J., Nixon, C. A., Flasar, F. M., et al. (2013). Strong temporal variability over one Saturnian year: From Voyager to Cassini. *Scientific Reports*, *3*(1), 1–5. https://doi.org/10.1038/srep02410

Li, L., Conrath, B. J., Flasar, F. M., & Gierasch, P. J. (2007). Revisit of the thermal wind equation: Application to planetary atmospheres at low latitudes. *Eos, Transactions of the American Geophysical Union*, *88*(24), P41A-0208.

Li, L., Gierasch, P. J., Achterberg, R. K., Conrath, B. J., Flasar, F. M., Vasavada, A. R., et al. (2008). Strong jet and a new thermal wave in Saturn's equatorial stratosphere. *Geophysical Research Letters*, *35*, L23208. https://doi.org/10.1029/2008GL035515

Li, L., Ingersoll, A. P., Vasavada, A. R., Porco, C. C., Del Genio, A. D., & Ewald, S. P. (2004). Life cycles of spots on Jupiter from Cassini images. *Icarus*, *172*(1), 9–23. https://doi.org/10.1016/j.icarus.2003.10.015

Li, L., Ingersoll, A. P., Vasavada, A. R., Simon-Miller, A. A., Del Genio, A. D., Ewald, S. P., et al. (2006). Vertical wind shear on Jupiter from Cassini images. *Journal of Geophysical Research*, *111*, E04004. https://doi.org/10.1029/2005JE002556

Li, L., Jiang, X., Ingersoll, A. P., del Genio, A. D., Porco, C. C., West, R. A., et al. (2011). Equatorial winds on Saturn and the stratospheric oscillation. *Nature Geoscience*, *4*(11), 750–752. https://doi.org/10.1038/NGEO1292

Limaye, S. S. (1986). Jupiter: New estimates of the mean zonal flow at the cloud level. *Icarus*, *65*(2-3), 335–352. https://doi.org/10.1016/0019-1035(86)90142-9

Momary, T. W., Baines, K. H., & the Cassini/VIMS Science Team (2006). The zoology of Saturn: The bizarre features unveiled by the 5 micron eyes of Cassini/VIMS. *Bulletin of the American Astronomical Society*, *38*, 499.

Pedlosky, J. (1987). *Geophysical fluid dynamics*. New York: Springer-Verlag Press. https://doi.org/10.1007/978-1-4612-4650-3

Perez-Hoyos, S., & Sanchez-Lavega, A. (2006a). On the vertical wind shear of Saturn's equatorial jet at cloud level. *Icarus*, *180*(1), 161–175. https://doi.org/10.1016/j.icarus.2005.07.011

Perez-Hoyos, S., & Sanchez-Lavega, A. (2006b). Solar flux in Saturn's atmosphere: Penetration and heating rates in the aerosol and cloud layers. *Icarus*, *180*(2), 368–378. https://doi.org/10.1016/j.icarus.2005.10.009

Porco, C. C., Baker, E., Barbara, J., Beurle, K., Brahic, A., Burns, J. A., et al. (2005). Cassini imaging science: Initial results on Saturn's atmosphere. *Science*, *307*(5713), 1243–1247. https://doi.org/10.1126/science.1107691

Porco, C. C., West, R. A., Squyres, S., Mcewen, A., Thomas, P., Murray, C. D., et al. (2004). Cassini imaging science: Instrument characteristics and anticipated scientific investigations at Saturn. *Space Science Reviews*, *115*(1-4), 363–497. https://doi.org/10.1007/s11214-004-1456-7

Read, P. L., Conrath, B. J., Fletcher, L. N., Gierasch, P. J., Simon-Miller, A. A., & Zuchowski, L. C. (2009). Mapping potential vorticity dynamics on Saturn: Zonal mean circulation from Cassini and Voyager data. *Planetary and Space Science*, *57*(14-15), 1682–1698. https://doi.org/10.1016/j.pss.2009.03.004

Read, P. L., Dowling, T. E., & Schubert, G. (2009). Saturn's rotation period from its atmospheric planetary-wave configuration. *Nature*, *460*, 608–610.

Read, P. L., Fletcher, L. N., Irwin, P. G. J., Barney, J. G., & Achterberg, R. (2007). Zonal mean dynamics on Saturn from Cassini and Voyager data. *Bulletin of the American Astronomical Society*, *39*, 487.

Sanchez-Lavega, A., García-Melendo, E., Pérez-Hoyos, S., Hueso, R., Wong, M. H., Simon, A., et al. (2016). An enduring rapidly moving storm as a guide to Saturn's equatorial jet complex structure. *Nature Communications*, *7*, 1–10. https://doi.org/10.1038/ncomms13262

Sayanagi, K. M., Dyudina, U. A., Ewald, S. P., Fischer, G., Ingersoll, A. P., Kurth, W. S., et al. (2013). Dynamics of Saturn's great storm of 2010–2011 from Cassini ISS and RPWS. *Icarus*, *223*(1), 460–478. https://doi.org/10.1016/j.icarus.2012.12.013

Simon, A. A., Li, L., & Reuter, D. C. (2015). Small-scale waves on Jupiter: A reanalysis of New Horizons, Voyager, and Galileo data. *Geophysical Research Letters*, *42*, 2612–2618. https://doi.org/10.1002/2015GL063433

Simon-Miller, A. A., Conrath, B., Gierasch, P., Orton, G., Achterberg, R., Flasar, F., & Fisher, B. (2006). Jupiter's atmospheric temperatures: From Voyager IRIS to Cassini CIRS. *Icarus*, *180*(1), 98–112. https://doi.org/10.1016/j.icarus.2005.07.019

Sromovsky, L. A., & Fry, P. M. (2010). The source of widespread 3-μm absorption in Jupiter's clouds: Constraints from 2000 Cassini VIMS observations. *Icarus*, *210*(1), 230–257. https://doi.org/10.1016/j.icarus.2010.06.039

Tomasko, M. G., & Doose, L. R. (1984). Polarimetry and photometry of Saturn from Pioneer 11: Observations and constraints on the distribution and properties of cloud and aerosol particles. *Icarus*, *58*(1), 1–34. https://doi.org/10.1016/0019-1035(84)90096-4

Trammell, H. J., Li, L., Jiang, X., Pan, Y., Smith, M. A., Bering, E. A., et al. (2016). Vortices in Saturn's northern hemisphere (2008–2015) observed by Cassini ISS. *Journal of Geophysical Research: Planets*, *121*, 1814–1826. https://doi.org/10.1002/2016JE005122

Trammell, H. J., Li, L., Jiang, X., Smith, M., Horst, S., & Vasavada, A. (2014). The global vortex analysis of Jupiter and Saturn based on Cassini imaging science subsystem. *Icarus*, *242*, 122–129. https://doi.org/10.1016/j.icarus.2014.07.019

Vasavada, A. R., Horst, S. M., Kennedy, M. R., Ingersoll, A. P., Porco, C. C., Del Genio, A. D., & West, R. A. (2006). Cassini imaging of Saturn: Southern hemisphere winds and vortices. *Journal of Geophysical Research*, *111*, E05004. https://doi.org/10.1029/2005JE002563

West, R. A. (1983). Spatially resolved methane band photometry of Saturn: II. Cloud structure models at four latitudes. *Icarus*, *53*(2), 301–309. https://doi.org/10.1016/0019-1035(83)90150-1